AD-A127 328 FATIGUE CRACK GROWTH AND SURFACE REACTIONS FOR TITANIUM 1/
ALLOYS EXPOSED TO..(U) LEHIGH UNIV BETHLEHEM PA INST OF
FRACTURE AND SOLID MECHANICS.. S J GAO ET AL. MAR 83
UNCLASSIFIED IFSM-83-116 N00014-75-C-0543 F/G 11/6 NL

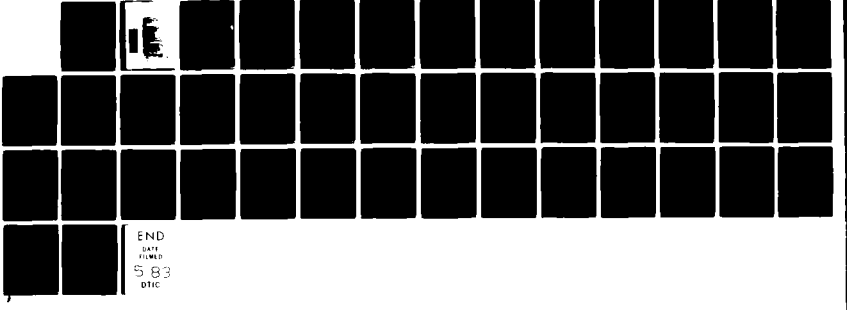

END
DATE FILMED
5 83
DTIC

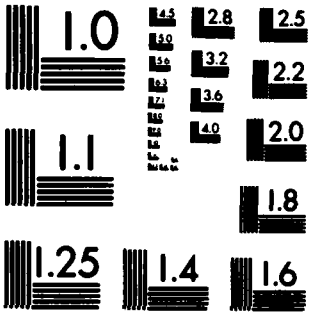

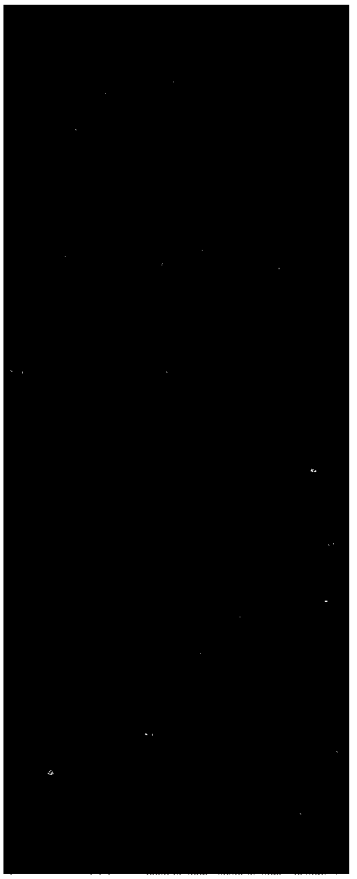

12

FATIGUE CRACK GROWTH AND SURFACE REACTIONS FOR TITANIUM ALLOYS EXPOSED TO WATER VAPOR

by

S. J. Gao[1], G. W. Simmons[2] and R. P. Wei[3]
LEHIGH UNIVERSITY
Bethlehem, PA 18015

March, 1983

Technical Report No. 14

OFFICE OF NAVAL RESEARCH
(Contract N00014-75-C-0543, NR036-097)

[1] Visiting Scholar. Shenyang Metals Research Institute, Academica Sinica, Shenyang, Peoples' Republic of China.
[2] Professor of Chemistry, Department of Chemistry.
[3] Professor of Mechanics, Department of Mechanical Engineering and Mechanics

Unclassified

SECURITY CLASSIFICATION OF THIS PAGE (When Data Entered)

REPORT DOCUMENTATION PAGE	READ DISTRIBUTIONS BEFORE COMPLETING FORM
1. REPORT NUMBER: IFSM-83-116	2. GOVT ACCESSION NO.: AD-A127328 / 3. RECIPIENT'S CATALOG NUMBER
4. TITLE (and Subtitle): FATIGUE CRACK GROWTH AND SURFACE REACTIONS FOR TITANIUM ALLOYS EXPOSED TO WATER VAPOR	5. TYPE OF REPORT & PERIOD COVERED: Technical Report No. 14
	6. PERFORMING ORG. REPORT NUMBER
7. AUTHOR(s): S. J. Gao, G. W. Simmons and R. P. Wei	8. CONTRACT OR GRANT NUMBER(s): Contract N00014-75-C-0543
9. PERFORMING ORGANIZATION NAME AND ADDRESS: Lehigh University, Bethlehem, PA 18015	10. PROGRAM ELEMENT, PROJECT, TASK AREA & WORK UNIT NUMBERS: NR 036-097
11. CONTROLLING OFFICE NAME AND ADDRESS: Office of Naval Research, Department of the Navy, Arlington, VA	12. REPORT DATE: March, 1983
	13. NUMBER OF PAGES: 41
14. MONITORING AGENCY NAME & ADDRESS(if different from Controlling Office)	15. SECURITY CLASS. (of this report): Unclassified
	15a. DECLASSIFICATION/DOWNGRADING SCHEDULE

16. DISTRIBUTION STATEMENT (of this Report)

This document has been approved for public release and sale; its distribution is unlimited.

17. DISTRIBUTION STATEMENT (of the abstract entered in Block 20, if different from Report)

18. SUPPLEMENTARY NOTES

19. KEY WORDS (Continue on reverse side if necessary and identify by block number)

Fatigue crack growth; surface reactions; titanium alloy; fracture mechanics; surface chemistry; water vapor.

20. ABSTRACT (Continue on reverse side if necessary and identify by block number)

Parallel fracture mechanics and surface chemistry studies have been carried out to develop understanding of environmentally assisted fatigue crack growth in titanium alloys. Room temperature crack growth response in water vapor was determined for annealed Ti-5Al-2.5Sn alloy and for Ti-6Al-4V alloy in the solution treated and solution treated plus over-aged conditions as a function of water vapor pressure from 0.266 to 665 Pa at a frequency of 5 Hz and a load ratio of 0.1. Reference data were

DD FORM 1 JAN 73 1473 EDITION OF 1 NOV 65 IS OBSOLETE

Unclassified

SECURITY CLASSIFICATION OF THIS PAGE (When Data Entered)

obtained in vacuum. The kinetics of reactions of water vapor and oxygen with fresh surfaces of Ti-5Al-2.5Sn alloy were measured at room temperature.

The results showed that the the reactions with water vapor and with oxygen are both rapid; with an initial sticking coefficient of 1.0 for water vapor and of 0.54 to 0.84 for oxygen. The reaction with water vapor produced a monolayer of oxide (TiO), whereas 2 to 3 layers of TiO resulted from the reaction with oxygen. Enhancement of fatigue crack growth by water vapor is believed to result from embrittlement by hydrogen that is produced by the reaction of water vapor with the fresh crack surfaces. Fatigue crack growth response was shown tc conform to a model for transport controlled crack growth.

FATIGUE CRACK GROWTH AND SURFACE REACTIONS FOR TITANIUM ALLOYS EXPOSED TO WATER VAPOR

S. J. Gao[1], G. W. Simmons[2] and R. P. Wei[3]
LEHIGH UNIVERSITY
Bethlehem, PA 18015

ABSTRACT

Parallel fracture mechanics and surface chemistry studies have been carried out to develop understanding of environmentally assisted fatigue crack growth in titanium alloys. Room temperature crack growth response in water vapor was determined for annealed Ti-5Al-2.5Sn alloy and for Ti-6Al-4V alloy in the solution treated and solution treated plus over-aged conditions as a function of water vapor pressure from 0.266 to 665 Pa at a frequency of 5 Hz and a load ratio of 0.1. Reference data were obtained in vacuum. The kinetics of reactions of water vapor and oxygen with fresh surfaces of Ti-5Al-2.5Sn alloy were measured at room temperature.

The results showed that the the reactions with water vapor and with oxygen are both rapid; with an initial sticking coefficient of 1.0 for water vapor and of 0.54 to 0.84 for oxygen. The reaction with water vapor produced a monolayer of oxide (TiO), whereas 2 to 3 layers of TiO resulted from the reaction with oxygen. Enhancement of fatigue crack growth by water vapor is believed to result from embrittlement by hydrogen that is produced by the reaction of water vapor with the fresh crack surfaces. Fatigue crack growth response was shown to conform to a model for transport controlled crack growth.

---

[1]Visiting Scholar. Shenyang Metals Research Institute, Academica Sinica, Shenyang, Peoples' Republic of China.

[2]Professor of Chemistry, Department of Chemistry.

[3]Professor of Mechanics, Department of Mechanical Engineering and Mechanics.

FATIGUE CRACK GROWTH AND SURFACE REACTIONS FOR TITANIUM ALLOYS EXPOSED TO WATER VAPOR

S. J. Gao, G. W. Simmons and R. P. Wei
LEHIGH UNIVERSITY
Bethlehem, PA 18015

INTRODUCTION

Environmentally assisted subcritical crack growth in structural materials is of great importance, because in many cases these materials are exposed to deleterious environments which can cause embrittlement. The embrittlement sequence involves a number of processes. For a gaseous environment, the processes include gas phase transport, physical adsorption, dissociative chemical adsorption, entry, diffusion and the embrittlement reaction itself [1]. The process that governs subcritical crack growth in a specific material-environment system is dependent on the relative rates of these processes. Methods to identify the rate controlling process for crack growth have been developed through coordinated fracture mechanics and surface chemistry studies. Experimental results have shown that crack growth under sustained or cyclic load is controlled by gas transport in some cases (e.g., for 2219-T851 aluminum alloy in water vapor [2], AISI 4340 steel and A542 steel in low pressure hydrogen sulfide [3,4]), or by surface reactions in other cases (e.g., AISI 4340 steel in water or water vapor [5,6] and in hydrogen [7,8]), or by diffusion of hydrogen through the metal in still others (e.g., AISI 4340 steel exposed to a higher pressure of hydrogen sulfide [3]).

A model has been proposed that formalizes the relationship between environmentally assisted fatigue crack growth and the gas phase transport and surface reaction processes [9,10]. If the rate of surface reaction is fast relative to the rate of transport, fatigue crack growth is determined by gas transport. In this case, the model predicts that the corrosion fatigue component of fatigue crack growth rate, $(da/dN)_{cf}$, is a linear function of exposure $(p_o/2f)$, for $p_o/2f$ less than a critical value $(p_o/2f)_s$ (where p_o and f are the gas pressure and loading frequency, respectively). When $p_o/2f$ is equal to and greater than $(p_o/2f)_s$, $(da/dN)_{cf}$ reaches and remains at a saturation value, $(da/dN)_{cf,s}$. These predictions are substantiated by experimental results on 2219-T851 aluminum alloy tested in water vapor [2] and on A542 steel tested in hydrogen sulfide [4].

Like other structural materials, titanium alloys are often used in enviroments that contain moisture. Therefore, it is important to develop an understanding of subcritical crack growth response and to identify the controlling process for crack growth of titanium alloys exposed to water vapor. Since the reactions of water vapor with titanium are very fast, studies of crack growth kinetics and surface reactions can be used to further examine the model for transport controlled fatigue crack growth [9,10].

Fatigue crack growth experiments were carried out on a Ti-6Al-4V alloy in the solution treated and the solution treated plus over-aged condition, and on an annealed Ti-5Al-2.5Sn alloy. Crack growth kinetics were determined at room temperature as a

function of water vapor pressure, from 0.266 to 665 Pa. The kinetics for the surface reactions of water vapor and of oxygen with Ti-5Al-2.5Sn alloy at room temperature were also determined. The crack growth results are correlated with the measured surface reaction kinetics and are discussed in terms of the model for transport controlled fatigue crack growth.

MATERIAL AND EXPERIMENTAL WORK

Fatigue Crack Growth

Two 6.35 mm thick plates of Ti-6Al-4V alloy were used in the crack growth studies. Specimen blanks were cut from the plates and were given one of two heat treatments; namely, solution treated (ST) and solution treated plus over-aged (STOA). The solution treatment (ST) consisted of solution annealing at 1227 K (1750 F) for 10 min. in vacuum, followed by cooling in air. The STOA condition was obtained by solution annealing at 1227 K (1750 F) for 10 min. in vacuum and water quenching, followed by aging at 950 K (1250 F) for 4 h in vacuum and cooling in air. Longitudinal tensile properties for these plates are given in Table 1.

The Ti-5Al-2.5Sn alloy was received as a 25.4 mm thick plate in the mill annealed condition. To ensure an all α-phase structure, it was re-heat-treated by annealing in vacuum at 1173 K (1650 F) for 1 h and cooling in air. Auxiliary x-ray diffraction test revealed no trace of β-phase. Longitudinal tensile properties of this alloy are also given in Table 1.

TABLE 1: Longitudinal Tensile Properties of Titanium Alloys (Averages of 3 Tests)

Alloy	Heat Treatment	Yield Strength (MPa)	Tensile Strength (MPa)	Elongation in 50.8 mm (pct)
Ti-6Al-4V	ST	833	911	12.3
Ti-6Al-4V	STOA	838	905	14.8
Ti-5Al-2.5Sn	Annealed	876	917	15.0

Wedge-opening-load (WOL) specimens, with thickness = 6.35 mm, width = 52.3 mm and half-height to width ratio (H/W) = 0.486, were used. For the Ti-6Al-4V alloy, the specimens were oriented with the crack plane perpendicular to the rolling direction and the crack growth direction in the long-transverse direction of the plates (i.e., the LT orientation). For the Ti-5Al-2.5Sn specimens, the TL orientation was selected. An initial (or crack starter) notch, 15.2 mm in length, was introduced into each specimen by electrodischarge machining. Each specimen was precracked in fatigue, while exposed to the test environment through a decreasing sequence of loads that terminated at the load level corresponding to the specified initial K for the actual experiment. The precracking procedure provided a fatigue crack about 3.2 mm in length from the starter notch, or a crack length of 18.4 mm, at the start of each experiment. This precracking procedure ensured that the subsequent fatigue crack growth would be through material that had not been altered by the notch preparation procedure, and would be unaffected by the starter notch geometry.

Fatigue crack growth experiments were carried out in vacuum and in water vapor at room temperature. The tests were carried out under constant-load-amplitude, sinusoidal loading in an automated closed-loop electrohydraulic testing machine operated in load control. Load control was estimated to be better than ±1 pct. A frequency of 5 Hz and a load ratio (R) of 0.1 were used. The tests coverd stress intensity factor range (ΔK) from about 14 MPa-$m^{1/2}$ to about 55 MPa-$m^{1/2}$. Stress intensity factor K for the WOL specimens was computed from Eqn. (1) [11]:

$$K = (Pa^{1/2}/BW)[30.96 - 195.8(a/W) + 730.6(a/W)^2 - 1186.3(a/W)^3 + 754.6(a/W)^4] \quad (1)$$

where P = applied load, B = specimen thickness, W = specimen width and a = crack length. Both specimen width and crack length are measured from the line of loading.

Tests were performed inside a modified commercial ultrahigh vacuum chamber using a static environment. Experiments in vacuum were made at pressures below 7 x 10^{-7} Pa, and those in water vapor by back-filling the chamber with water vapor from a high-purity source attached to the chamber. Purification was achieved through alternate freezing and thawing triply distilled water in the source and pumping away the dissolved gases. Prior to each experiment, the chamber was baked out and evacuated to about 7 x 10^{-7} Pa. Water vapor was then admitted into the chamber to the prescribed pressure. Pressure was monitored by a capacitance manometer. The tests covered water vapor pressures from 0.266 to 665 Pa (0.002 to 5 torr).

Crack length was measured with an ac electrical potential system [12,13]. Calibration tests were made to obtain an empirical relationship between crack length and electrical potential. These tests were accomplished by comparing electrical potential measurements against fatigue markings on fracture surfaces produced by intentionally introduced overloads during fatigue in air. Corrections for crack front curvature were made by measuring average crack lengths from the fatigue markings after specimen fracture. The following least-squares calibration equations were obtained from the results on two specimens:

$$a = 16.1 + 41.0V^{*}; \qquad \text{for } V^{*} \leq 0.286$$

$$a = 15.0 + 49.2V^{*} - 14.3V^{*2}; \qquad \text{for } 0.286 < V^{*} < 0.7$$

$$\text{(a in mm)} \qquad (2)$$

$V^{*} = (V - V_r)/V_r$ is the normalized potential, V is the potential corresponding to crack length a, and V_r is the reference potential corresponding to the initial notch. With a working current of 0.75A (*rms*) at 93 Hz, the accuracy and the resolution of crack length measurement were estimated to be 1.3 pct and 15 μm, respectively, for the WOL specimens used in this study.

Surface Reactions

Auger electron spectroscopy (AES) was used to determine the kinetics of reactions of water vapor and oxygen with titanium alloy surfaces at room temperature. The measurements were limited to the Ti-5Al-2.5Sn alloy. Clean surfaces produced by *in situ* impact fracture of notched round specimens were used. Exposures of these surfaces to water vapor and to oxygen were

achieved by back-filling the spectrometer chamber from high purity water and oxygen sources. High purity water vapor was obtained by alternately freezing and thawing triply distilled water contained in a side arm to the spectrometer chamber, and pumping away the dissolved gases. The oxygen was contained in a one-liter Pyrex bulb, and was of 99.95 pct purity.

For the surface studies, background pressure in the spectrometer chamber was typically of the order of 6.7×10^{-8} Pa (5×10^{-10} torr), as measured by an ionization gage. The reactant gases were admitted into the chamber to pressures below 1.3×10^{-4} Pa (10^{-6} torr) to effect the desired exposures. The chamber was re-evacuated to below 6.7×10^{-7} Pa (5×10^{-9} torr) prior to each analysis. At these low pressures (i.e., below 1.3×10^{-4} Pa), reactions induced by species created by the ionization gage filament and by the incident electron beam were minimal. A different area of the impact fracture surface was analyzed for each exposure, using a scanning Auger microprobe (SAM), to preclude the inclusion of any effects that might have been induced by the incident beam during the previous measurements.

The extent of reactions of water vapor and oxygen with the alloy surface was determined by measuring the oxygen Auger electron peak-to-peak height (APPH) as a function of exposure (pressure x time). To compare the results of several different experiments, the oxygen Auger electron signal (measured for constant instrumental parameters) was normalized with respect to the APPH of the Ti(387 eV) signal for a clean titanium surface.

The Ti(418 eV) transition is sensitive to changes in matrix, since this transition involves the valence band. The changes in the valence-level density of states that occur upon oxidation give rise to significant changes in the shape of the Ti(418 eV) peak. Changes in the shape of this peak, therefore, were used to detect the onset of oxidation, and the characteristic peak shapes were used to identify the oxide phases.

RESULTS

Fatigue Crack Growth Response

Room temperature fatigue crack growth data for solution treated (ST) and solution treated plus over-aged (STOA) Ti-6Al-4V alloys are shown as a function of stress intensity factor range (ΔK) in Figs. 1 and 2, respectively. These data indicate that the fatigue crack growth rates in water vapor are faster than those in vacuum, especially in the lower ΔK region. The influence of water vapor in the higher ΔK region is relatively small. The effect of water vapor pressure on fatigue crack growth rate can be seen also in Figs. 1 and 2. The pressure dependence is characterized by the fact that the rates of fatigue crack growth increase with increasing pressure below a critical or saturation pressure, reaching a maximum value and remain unchanged beyond the critical pressure. This behavior is discussed on the basis of the transport controlled crack growth model [9,10] in the following section.

Comparison of data for the Ti-6Al-4V alloy in the ST and STOA conditions is shown in Fig. 3. Crack growth rates in vacuum are the same for the two heat treatment conditions. The rates

for the solution treated (ST) alloy in water vapor, however, are slightly higher than those for the solution treated plus over-aged (STOA) alloy. It is noted that the strengths of Ti-6Al-4V alloy for these two heat treatments are nearly identical (see Table 1). The change in fatigue crack growth rates in water vapor for the two heat treatments, therefore, is believed to result from differences in microstructure rather than tensile or yield strength.

Results for the Ti-5Al-2.5Sn alloy are shown in Fig. 4. It is seen that water vapor also enhanced fatigue crack growth rates, but its effect disappeared at ΔK values above about 30 MPa-$m^{1/2}$.

Surface Reaction Kinetics

Auger electron spectra of the impact fracture surface of Ti-5Al-2.5Sn alloy, Fig. 5a, indicate the presence of only the alloying elements; (the aluminum Auger peak at 1400 eV is not shown). Typical changes in the spectra after exposure of the fracture surface to water vapor and to oxygen are shown in Figs. 5b and 5c, respectively. The reaction kinetics of these gases with the clean alloy surface are shown in terms of normalized oxygen Auger peak intensities, or APPH, versus exposure in Fig. 6 for water vapor and in Fig. 7 for oxygen. For the reaction with oxygen, a saturation value is reached following an exposure of 4×10^{-3} to 5.3×10^{-3} Pa-s (3×10^{-5} to 4×10^{-5} torr-s). In the case of reactions with water vapor, an apparent initial saturation is reached after approximately 10^{-3} to 1.3×10^{-3} Pa-s (8×10^{-6} to 10^{-5} torr-s) exposure. The normalized oxygen APPH

for this initial saturation in water vapor is about one-half that of the saturation level achieved in oxygen. Beyond this initial saturation, however, there was a further, but slower, reaction of water vapor with the titanium alloy surface.

Comparison of the Ti(418 eV) peak from the clean surface, Fig. 5a, with the corresponding peak after 5.3×10^{-3} Pa-s (4×10^{-5} torr-s) exposure to water vapor and to oxygen, Figs. 5b and 5c, shows changes in the titanium Auger electron transitions. Changes in the Ti(418 eV) peak after 5.3×10^{-3} Pa-s exposure to oxygen are significant and suggest oxidation of the surface even for this modest exposure. The shape of the Ti(418 eV) peak is similar to that reported by Solomon and Baun [14] for bulk TiO, with a characteristic small peak at about 405 eV. There are smaller, but demonstrable changes in the Ti(418 eV) peak after 5.3×10^{-3} Pa-s exposure to water vapor which indicate the possible initiation of oxidation.

Fracture surfaces produced by sustained-load crack growth in 1.33 kPa (10 torr) water vapor inside the Auger spectrometer chamber, using methods described in [15], were also analyzed, Fig. 5d. The relative oxygen-to-titanium signal and the energy distribution of the titanium peaks, following this high exposure to water vapor, are similar to the corresponding features in the spectra for oxygen, Fig. 5c. The indicated extent of reaction with the fracture surface is consistent with the apparent further reactions with water vapor beyond the initial saturation level, Fig. 6.

DISCUSSION

The rate and extent of reactions of water vapor with titanium alloys are of primary interest for the interpretation of results on environmentally assisted fatigue crack growth. The results for oxygen are included for the purpose of comparison and background for future studies of the inhibition of crack growth by oxygen [10]. Before considering their relationships to crack growth response, quantitative estimates of the kinetics of surface reactions from the AES data are discussed.

Surface Reactions

For water vapor, it will be shown later that the extent of reaction corresponding to the initial saturation level can be at most equivalent to one oxygen per surface titanium atom. In this case, the normalized oxygen signal may be expected to be approximately proportional to the amount of adsorbed oxygen up to the saturation level. For the initial reaction with water vapor, the following rate equation is assumed to apply:

$$d\theta/dt = (S_o/N_o)(2\pi mkT)^{-1/2}(1 - \theta) \qquad (3)$$

In Eqn. (3), θ is the coverage and is defined as n/N_o, where n is the surface concentration of oxygen at time t, and N_o is the surface oxygen concentration at saturation. S_o is the initial sticking coefficient, $p(2\pi mkT)^{-1/2}$ is the arrival rate of water molecules, and $(1 - \theta)$ is the fraction of unreacted surface. The rate constant, k_c, is thus $k_c = (S_o/N_o)(2\pi mkT)^{-1/2}$. Integration

of Eqn. (3) gives the following expression for θ in terms of the exposure pt:

$$\ln(1 - \theta) = - (S_o pt/N_o)(2\pi mkT)^{-1/2} \quad (4)$$

To calculate values of $\ln(1 - \theta)$, a representative value of the normalized oxygen signal for the saturation level needs to be chosen. Although this choice is somewhat arbitrary, a value was selected to provide good fit to the data over a range of exposures up to 1.6×10^{-3} Pa-s (1.2×10^{-5} torr-s). A plot of $\ln(1 - \theta)$ as a function of water vapor exposure, pt, is shown in Fig. 8. From this plot a value of $S_o/N_o = 7.8 \times 10^{-16}$ cm^2 is obtained, which corresponds to a reaction rate constant of 2.8×10^3 $(Pa\text{-}s)^{-1}$. If the maximum value for S_o of unity is assumed, then the maximum oxygen concentration at saturation is 1.2×10^{15} cm^{-2}. For comparison, the number of atoms at the surface of polycrystalline titanium is estimated to be 1.35×10^{15} cm^{-2}, and the oxygen concentration in the (001) face of TiO is 1.12×10^{15} cm^{-2}.

For the case of reactions with oxygen, it is necessary to consider the attenuation of oxygen Auger electrons in relating the normalized oxygen signal to the amount of adsorbed oxygen at the surface, because the reaction can involve more than one layer of oxide. An estimate of this attenuation is made by considering the signal from n layers of oxide:

$$I = I_o[1 + \Sigma \exp(-nd/L\cos\phi)] \quad (5)$$

In Eqn. (5), I_o is the signal from a single layer of oxide, d is the thickness of this layer, L is the mean free path of oxygen

Auger electrons in the oxide, and ϕ is the angle between the surface normal and the entrance aperture of the Auger analyzer.

Based on the results of reactions with water vapor obtained in this study, it is assumed that the normalized oxygen signal at saturation in water vapor (I_o = 1.0) corresponds to a monolayer of TiO. The thickness, d, of this layer is expected to be of the order of the oxygen ionic diameter in TiO, or d = 0.299 nm. The mean free path of oxygen Auger (510 eV) electrons is not known precisely, but is expected to be between 0.8 and 1.0 nm on the basis of values of mean free paths reported for electrons of this energy in a number of other materials. Calculated values of oxygen signal as a function of the number of layers of oxide are given in Table 2, for assumed mean free paths of 0.8 and 1.0 nm.

TABLE 2: Calculated Signal (I) from n Layers of Oxide

LAYERS	SIGNAL (L = 0.8 nm)	SIGNAL (L = 1.0 nm)
1	1.00	1.00
2	1.60	1.66
3	1.96	2.10
4	2.17	2.39
5	2.30	2.59
6	2.38	2.72
7	2.42	2.80
8	2.45	2.86
9	2.47	2.90
10	2.48	2.92

From the foregoing estimate, the initial saturation level for the reaction of oxygen with Ti-5Al-2.5Sn alloy (Fig. 7) would correspond to 2 to 3 layers of TiO (equivalent to 0.6 to 0.9 nm in thickness).

If the reaction of oxygen with the titanium alloy had taken place by a sequence of reactions, such as the rapid formation of a monolayer of chemically adsorbed oxygen or a monolayer of oxide followed by a slower increase in oxide thickness, one would expect to observe an inflection in the data of normalized oxygen signal vs. exposure shown in Fig. 7. The fact that there is no observable inflection suggests that the chemisorption and the oxidation reaction, leading to the formation 0.6 to 0.9 nm of oxide, have comparable rates. The rate of oxygen reaction can thus be described in terms of the rate of change in the area of surface that is occupied by the oxide overlayer with exposure. Equations (3) and (4) can be used for this purpose by redefining Θ as the areal fraction of surface covered by the 0.6 to 0.9 nm thick layer of oxide. A plot of $\ln(1 - \Theta)$ vs. exposure (pt) is shown in Fig. 9. A value of $S_o/N_o = 2.5 \times 10^{-16}$ cm^2 is obtained, which corresponds to a rate constant for this reaction of $k_c = 1.3 \times 10^3$ (Pa-s)$^{-1}$. The 0.6 to 0.9 nm thick oxide film, corresponding to the initial saturation level, would have an oxygen concentration on the order of 2.2×10^{15} to 3.4×10^{15} cm^{-2}. For these values of N_o, the corresponding values for the initial sticking coefficient, S_o, would be on the order of 0.54 to 0.84.

These results indicate that the reaction of water vapor with the titanium alloy surface takes place with an initial sticking coefficient on the order of unity, and reaches an initial

saturation level that is equivalent to a monolayer of oxide (i.e., TiO). There is apparently an additional, slower reaction with water vapor as evidenced by further changes in the Auger spectra for fracture surfaces exposed to 1.3 kPa (10 torr) of water vapor. The similarity between the spectra following this extensive exposure to water vapor and those for oxygen exposures of 0.0133 to 0.133 Pa-s (10^{-4} to 10^{-3} torr-s) suggests that the limiting thickness of oxide formed in water vapor approaches that formed at low exposures to oxygen.

The initial sticking coefficient for oxygen is estimated to be between 0.54 and 0.84, as compared to unity (or 1.0) for water vapor. The initial limiting thickness of oxide formed from the reaction of Ti-5Al-2.5Sn alloy with oxygen, on the other hand, is 2 to 3 times that formed with water vapor. The reactions and extent of reactions for Ti-5Al-2.5Sn alloy with water vapor and oxygen are in general agreement with studies of titanium surfaces [16-21]. These surface reaction results are considered in relation to environmentally assisted fatigue crack growth in the following discussions.

Fatigue Crack Growth

From the surface chemistry studies, it is seen that the surface reaction rate for water vapor with titanium alloy is very fast. The reaction rate constant at room temperature, k_c, calculated from the data in Figs. 6 and 8, is of the order 10^3 $(Pa\text{-}s)^{-1}$. (Although there is apparently a slower additional reaction, its contribution to crack growth appears to be small. No further consideration of this second reaction will be given

here.) The rate constant for the fast reaction is comparable to that for the reaction of water vapor with 2219-T851 aluminum alloy [2] and to that for the first step in the reactions of hydrogen sulfide with AISI 4340 steel [3]. For the latter two cases, fatigue crack growth has been identified as being controlled by the transport of deleterious gases to the crack tip [2,4]. Consequently, one can expect that, in the case of titanium alloys exposed to water vapor, fatigue crack growth would also be controlled by gas transport.

A model [9,12] for transport controlled fatigue crack growth has been developed and has been modified recently to account for the effect of load ratio [13]. The data obtained from this study may be used to further examine this crack growth model. According to the model [9,12,13], the rate of fatigue crack growth in a deleterious environment, $(da/dN)_e$, is composed of the sum of two rates -- the rate of growth in an inert reference environment or that of the "pure" (mechanical) fatigue component, $(da/dN)_r$, and the rate for the cycle-dependent environmental or "corrosion fatigue" component, $(da/dN)_{cf}$. (Here the contribution from stress corrosion cracking or sustained load growth is assumed to be negligible.) The component $(da/dN)_{cf}$ is assumed to be proportional to the amount of embrittling species (hydrogen) produced by the surface reaction during each loading cycle, and is thus proportional to the size of the "effective" reacting surface area and to the extent of surface reaction [9,12].

By assuming that the surface reaction follows Langmuir kinetics and that gas transport along the crack proceeds by Knudsen or molecular flow, the following relationships were

derived for transport controlled fatigue crack growth [9,12,13]:

$$\frac{(da/dN)_{cf}}{(da/dN)_{cf,s}} = \frac{(p_o/2f)}{(p_o/2f)_s} = 436\,\frac{\beta^*}{\alpha}\,\frac{\sigma_{ys}^2}{N_o kTE^2}\,\sqrt{T/M}\;f(R)\;(p_o/2f) \qquad (6)$$

$$(p_o/2f)_s \simeq \left[436\,\frac{\beta^*}{\alpha}\,\frac{\sigma_{ys}^2}{N_o kTE^2}\,\sqrt{T/M}\;f(R)\right]^{-1} \qquad (7)$$

$$f(R) = \frac{1}{4}\left[\left(\frac{1+R}{1-R}\right)^2 + \frac{1}{2}\right]; \quad \text{for sinusoidal loading and } 0 \le R < 1 \qquad (8)$$

In these equations, p_o = gas pressure of the surrounding environment, f = loading frequency, T = absolute temperature, k = Boltzmann's constant, M = molecular weight of the gas, N_o = density of surface sites for reaction, R = load ratio (i.e., ratio of minimum to maximum load in a given fatigue cycle), σ_{ys} = yield strength, and E = elastic modulus. The constants α and β^* are empirical constants relating to surface roughness and gas flow [9,12,13]. Subscript s is used here to denote the corresponding values at saturation. Equation (7) gives the value of $p_o/2f$ at which saturation in environmental effect can be expected; in other words, the combination of pressure and frequency (or exposure) for which the surface reaction is complete during one loading cycle. It can be seen from Eqn. (6) that the corrosion fatigue component of crack growth rate, $(da/dN)_{cf}$, varies linearly with $p_o/2f$ below saturation. When $p_o/2f$ is equal to and greater than $(p_o/2f)_s$, $(da/dN)_{cf}$ reaches and remains at the saturation value $(da/dN)_{cf,s}$.

A comparison of Eqn. (6) with the experimental results for Ti-6Al-4V alloy in water vapor is shown in Fig. 10. Data for the

two heat treatments at two different ΔK levels are used. The average value of available $(da/dN)_{cf}$ data at water vapor pressures of 13.3, 66.5, 266 and 665 Pa is used to represent the saturation value, $(da/dN)_{cf,s}$, for each ΔK level. Because $(da/dN)_{cf}$ is the difference between $(da/dN)_e$ and $(da/dN)_r$, which are of the same order of magnitude, errors for $(da/dN)_{cf}/(da/dN)_{cf,s}$ are expected to be very large, particularly at the lower water vapor pressures. The 95 pct confidence intervals were estimated from the residual standard deviations and are shown for each set of data in Fig. 10 [18]. The data indicate that the model is in good agreement with the experimental results.

In the model, β^*/α is taken to be an empirical constant and is to be determined from the fatigue crack growth data. By using the least-square method, the water vapor pressure $(p_o)_s$ at which the corrosion fatigue component of crack growth rate reaches the saturation value is found to be 2.2 Pa (0.016 torr) for a loading frequency of 5 Hz. Substitution of $(p_o)_s$ into Eqn. (7) gives a value of 3.7 for β^*/α for the Ti-6Al-4V alloys. The value of β^*/α determined from the experimental results for the Ti-6Al-4V alloy/water vapor system and from other material/environment systems are compared in Table 3. It appears that β^*/α is essentially a constant, and is independent of both the material and the environment. This observation along with the pressure dependence for the rate of fatigue crack growth lends further support for the model of transport controlled crack growth, and provides an indication of its broader applicability as an estimation procedure.

TABLE 3: The Empirical Constant β^*/α for Different Material and Environment Combinations

MATERIAL	ENVIRONMENT	β^*/α	REFERENCES
Ti-6Al-4V	Water Vapor	3.7	This Study
2219-T851	Water Vapor	3.8	[2,13]
2-1/4Cr-1Mo (A542, Class 2)	Hydrogen Sulfide	3.2	[4,9]

SUMMARY

Parallel fracture mechanics and surface chemistry studies have been carried out to develop understanding of environmentally assisted fatigue crack growth in titanium alloys. The room temperature fatigue crack growth responses have been determined for both solution treated (ST) and solution treated plus over-aged (STOA) Ti-6Al-4V alloys and for annealed Ti-5Al-2.5Sn alloy in water vapor at pressures from 0.266 to 665 Pa, as well as in vacuum. Tests were carried out at a frequency of 5 Hz and load ratio of 0.1, and covered stress intensity factor range (ΔK) from about 15 to 55 MPa-$m^{1/2}$. The experimental results showed that the rates of fatigue crack growth increased with increasing water vapor pressure until a critical pressure is reached, at which the growth rate attained a maximum (saturation) value.

The kinetics for the reactions of water vapor and oxygen with fresh surfaces of Ti-5Al-2.5Sn alloy at room temperature were determined. (The reactions with the Ti-6Al-4V alloy are expected to be similar.) The reactions were followed by

measuring changes in the oxygen Auger signal. The results showed that the reactions with water vapor and with oxygen are both rapid, with an initial sticking coefficient of 1.0 for water vapor and of 0.54 to 0.84 for oxygen. The reaction with water vapor resulted in the formation of a monolayer of oxide (TiO), whereas 2 to 3 layers of TiO resulted from the reaction with oxygen.

Based on the fracture mechanics and surface chemistry data, it appears that the enhancement of fatigue crack growth in the titanium alloys resulted from embrittlement by hydrogen that is produced by the reaction of newly created crack surfaces with water vapor. Crack growth is controlled by the rate of transport of water vapor to the crack tip, and the fatigue crack growth response conforms to and provides further confirmation for a model for transport controlled crack growth.

ACKNOWLEDGEMENT

Support of this research by the Office of Naval Research under Contract N00014-75-C-0543, NR 036-097 is gratefully acknowledged. Materials used in this study were made available by AFWAL; the assistance of A. Gunderson and Walt Griffith is very much appreciated. Assistance with heat treating the Ti-6Al-4V alloy by R. P. Gangloff of Exxon Corporate Research Laboratories is also acknowledged.

REFERENCES

1. D. P. Williams, P. S. Pao, and R. P. Wei, Environment-Sensitive Fracture of Engineering Materials, Z. A. Foroulis, ed., p. 3, The Met. Soc.-AIME, Warrendale, PA, 1979.

2. R. P. Wei, P. S. Pao, R. G. Hart, T. W. Weir, and G. W. Simmons, Met. Trans. A, 1980, vol. 11A, p. 151.

3. M. Lu, P. S. Pao, T. W. Weir, G. W. Simmons, and R. P. Wei, Met. Trans. A, 1981, vol. 12A, p. 805.

4. R. Brazill, G. W. Simmons, and R. P. Wei, J. Eng. Mater. Techn., 1979, vol. 101, p. 199.

5. G. W. Simmons, P. S. Pao, and R. P. Wei, Met. Trans. A, 1978, vol. 9A, p. 1147.

6. P. S. Pao, W. Wei, and R. P. Wei, Environment-Sensitive Fracture of Engineering Materials, Z. A. Foroulis, ed., p. 565, The Met. Soc.-AIME, Warrendale, PA, 1979.

7. M. Lu, P. S. Pao, N. H. Chan, K. Klier, and R. P. Wei, Hydrogen in Metals, Suppl. to Trans. Jpn. Inst. Metals, 1980, vol. 21, p. 449.

8. N. H. Chan, K. Klier, and R. P. Wei, Hydrogen in Metals, Suppl. to Trans. Jpn. Inst. Metals, 1980, vol. 21. p. 305.

9. T.W. Weir, G. W. Simmons, R. G. Hart, and R. P. Wei, Scr. Met., 1980, vol. 14, p. 357.

10. R. P. Wei and R. L. Brazill, "An AC Potential System for Crack Length Measurement", The Measurement of Crack Length and Shape During Fracture and Fatigue, C. J. Beevers, ed., Engineering Materials Advisory Services Ltd. (EMAS), Warley, England, 1980.

11. R. P. Wei and R. L. Brazill, in Fatigue Crack Growth Measurement and Data Analysis, ASTM STP 738, S. J. Hudak, Jr. and R. J. Bucci, eds., American Society for Testing and Materials, 1981, pp. 103-119.

12. R. P. Wei and G. W. Simmons, "Surface Reactions and Fatigue Crack Growth", Proceedings of 27th Sagamore Army Materials Research Conference, New York, July, 1980.

13. T. H. Shih, Thesis, Lehigh University, Bethlehem, PA, 1981.

14. B. Kasemo and E. Tornqvist, Surf. Sci., 1978, vol. 77, pp. 209-218.

15. T. Smith, Surf. Sci., 1973, vol. 38, pp. 292-312.

16. D.J. Harra, J. Vac. Sci. Technol., 1975, vol. 12, pp. 539-542.

17. D.J. Harra, J. Vac. Sci. Technol., 1976, vol. 13, pp. 471-474.

18. W.G. Clark, Jr. and S. J. Hudak, Jr., J. Test. and Eval., vol. 3, No. 6, Nov. 1975, pp. 454-476.

FIGURE CAPTIONS

Fig. 1: Influence of water vapor pressure on the kinetics of fatigue crack growth in solution treated Ti-6Al-4V alloy at room temperature.

Fig. 2: Influence of water vapor pressure on the kinetics of fatigue crack growth in solution treated plus over-aged Ti-6Al-4V alloy at room temperature.

Fig. 3: Comparison of data for Ti-6Al-4V alloy in the solution treated (ST) and solution treated plus over-aged (STOA) conditions.

Fig. 4: Influence of water vapor pressure on the kinetics of fatigue crack growth in Ti-5Al-2.5Sn alloy at room temperature.

Fig. 5: Auger electron spectra of Ti-5Al-2.5Sn surfaces: (a) after impact fracture in vacuum, (b) after exposure to 5.3×10^{-3} Pa-s (4×10^{-5} torr-s) water vapor, (c) after exposure to 5.3×10^{-3} Pa-s (4×10^{-5} torr-s) oxygen, and (d) after exposure to 1.33 kPa (10 torr) water vapor. (E_p = 2 keV, 3 eV peak to peak, I_p = 20 μA.)

Fig. 6: Normalized oxygen Auger electron signal versus water vapor exposure.

Fig. 7: Normalized oxygen Auger electron signal versus oxygen exposure.

Fig. 8: Plot of $\ell n\ (1 - \theta)$ as a function of water vapor exposure.

Fig. 9: Plot of $\ell n\ (1 - \theta)$ as a function of oxygen exposure.

Fig. 10: Comparison of normalized (corrosion) fatigue crack growth rates for Ti-6Al-4V alloy with model predictions for pressure dependence.

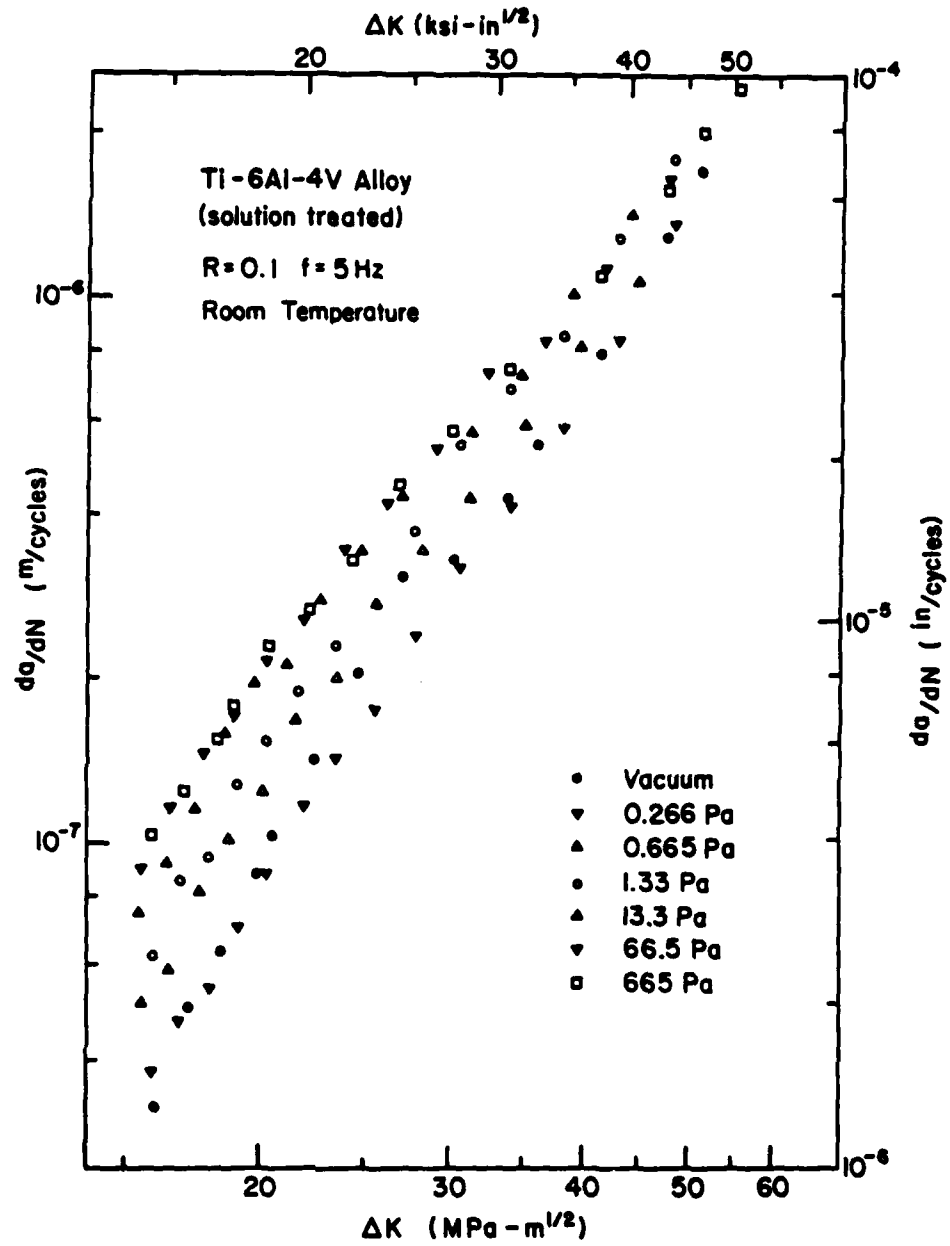

Fig. 1: Influence of water vapor pressure on the kinetics of fatigue crack growth in solution treated Ti-6Al-4V alloy at room temperature.

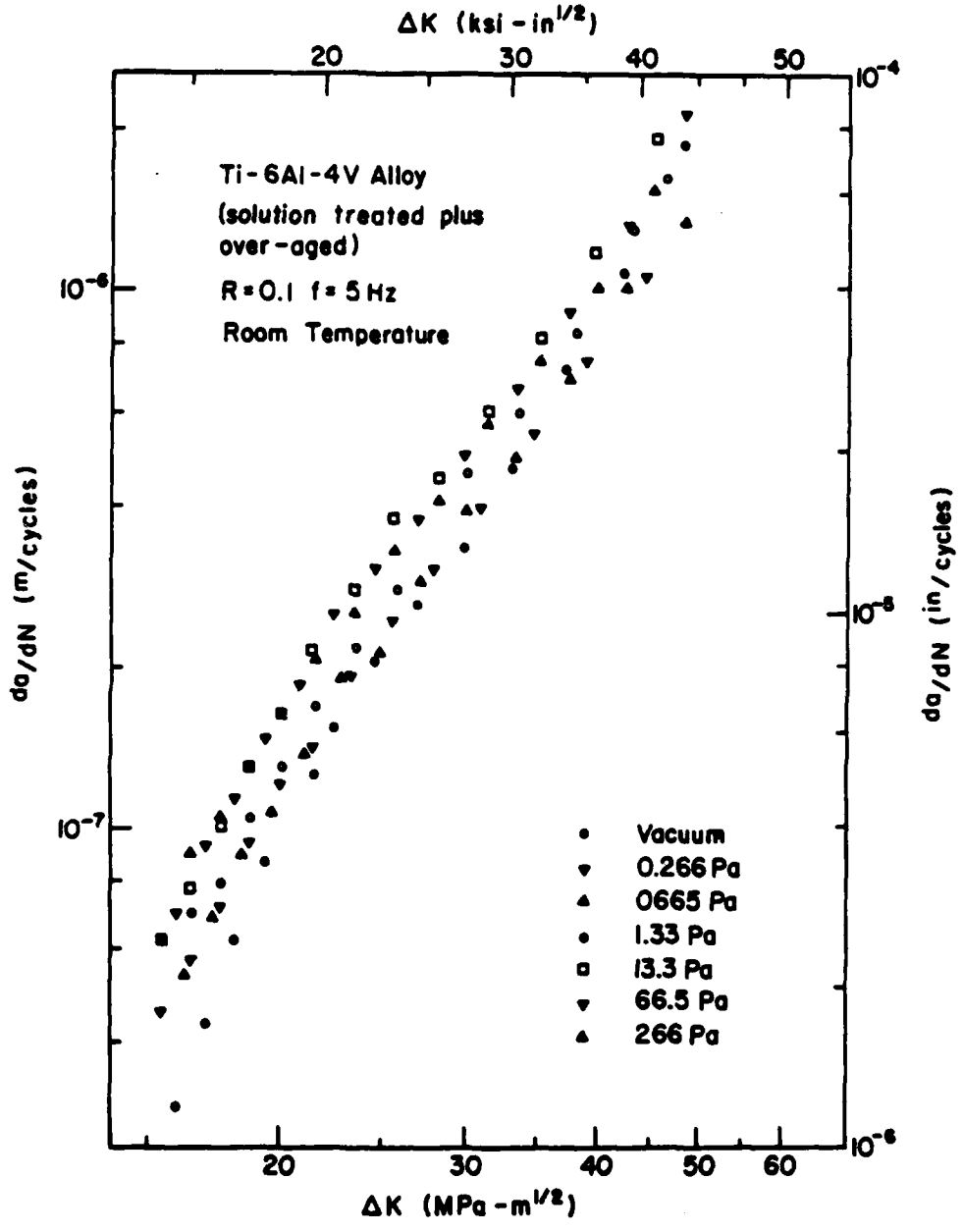

Fig. 2: Influence of water vapor pressure on the kinetics of fatigue crack growth in solution treated plus over-aged Ti-6Al-4V alloy at room temperature.

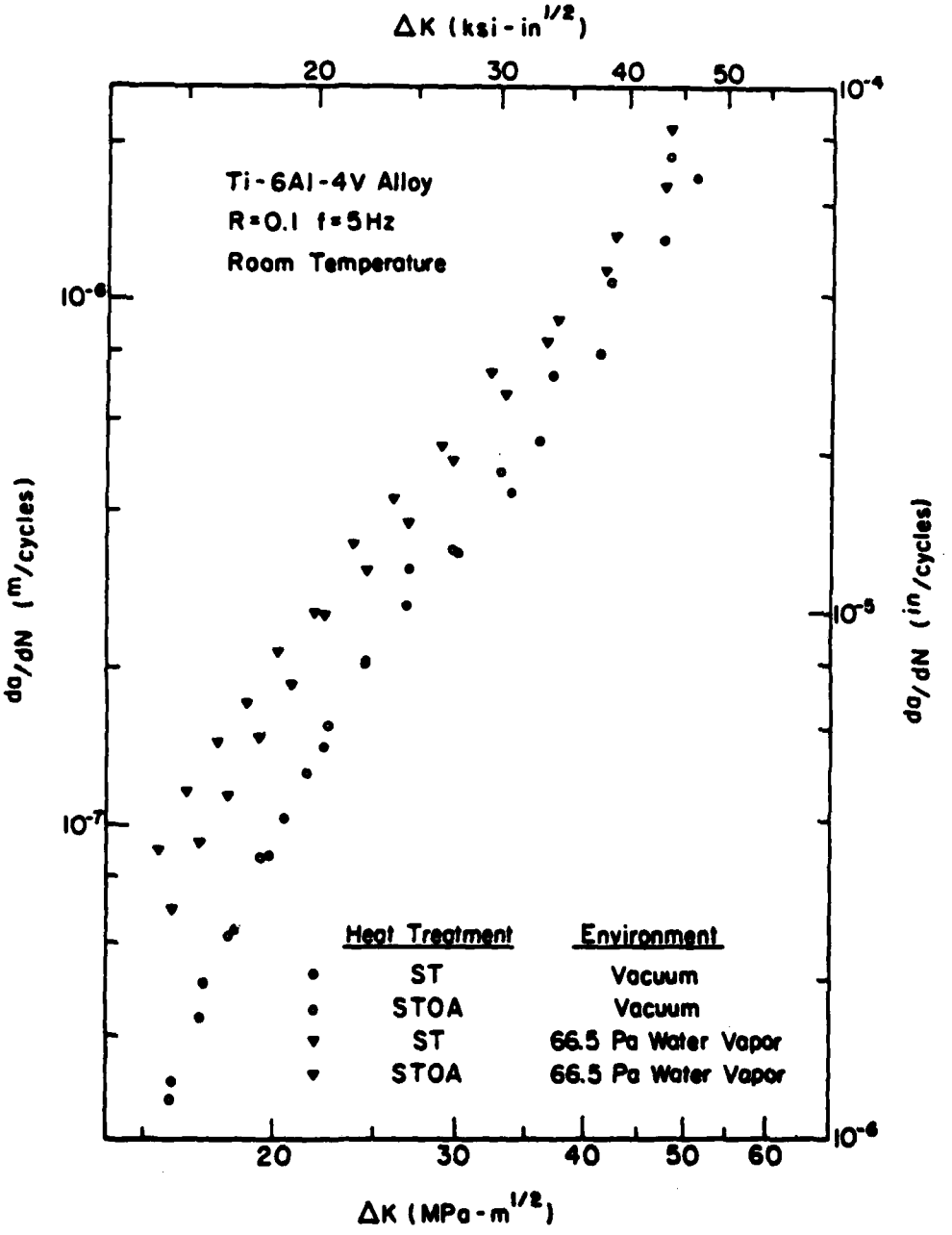

Fig. 3: Comparison of data for Ti-6Al-4V alloy in the solution treated (ST) and solution treated plus over-aged (STOA) conditions.

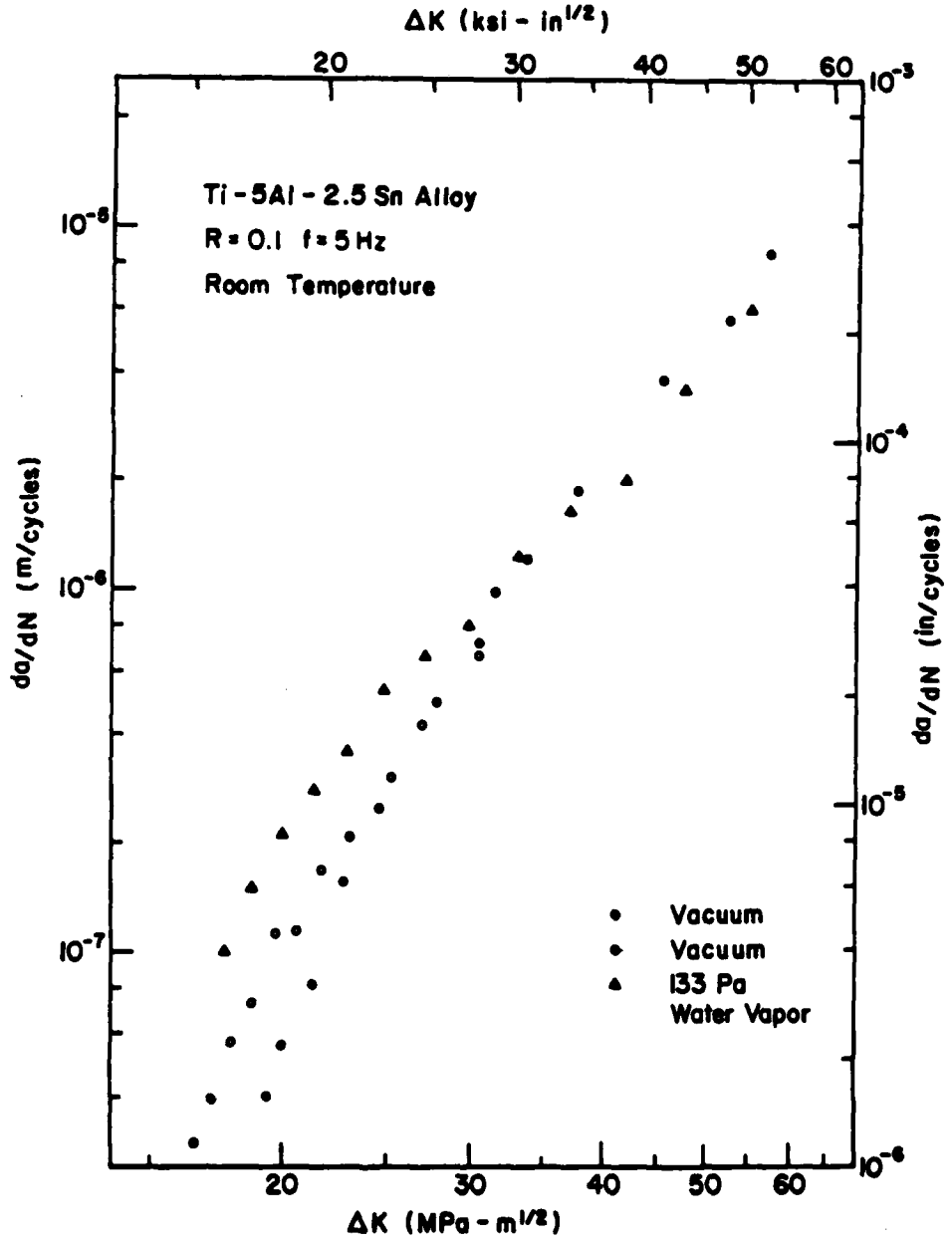

Fig. 4: Influence of water vapor pressure on the kinetics of fatigue crack growth in Ti-5Al-2.5Sn alloy at room temperature.

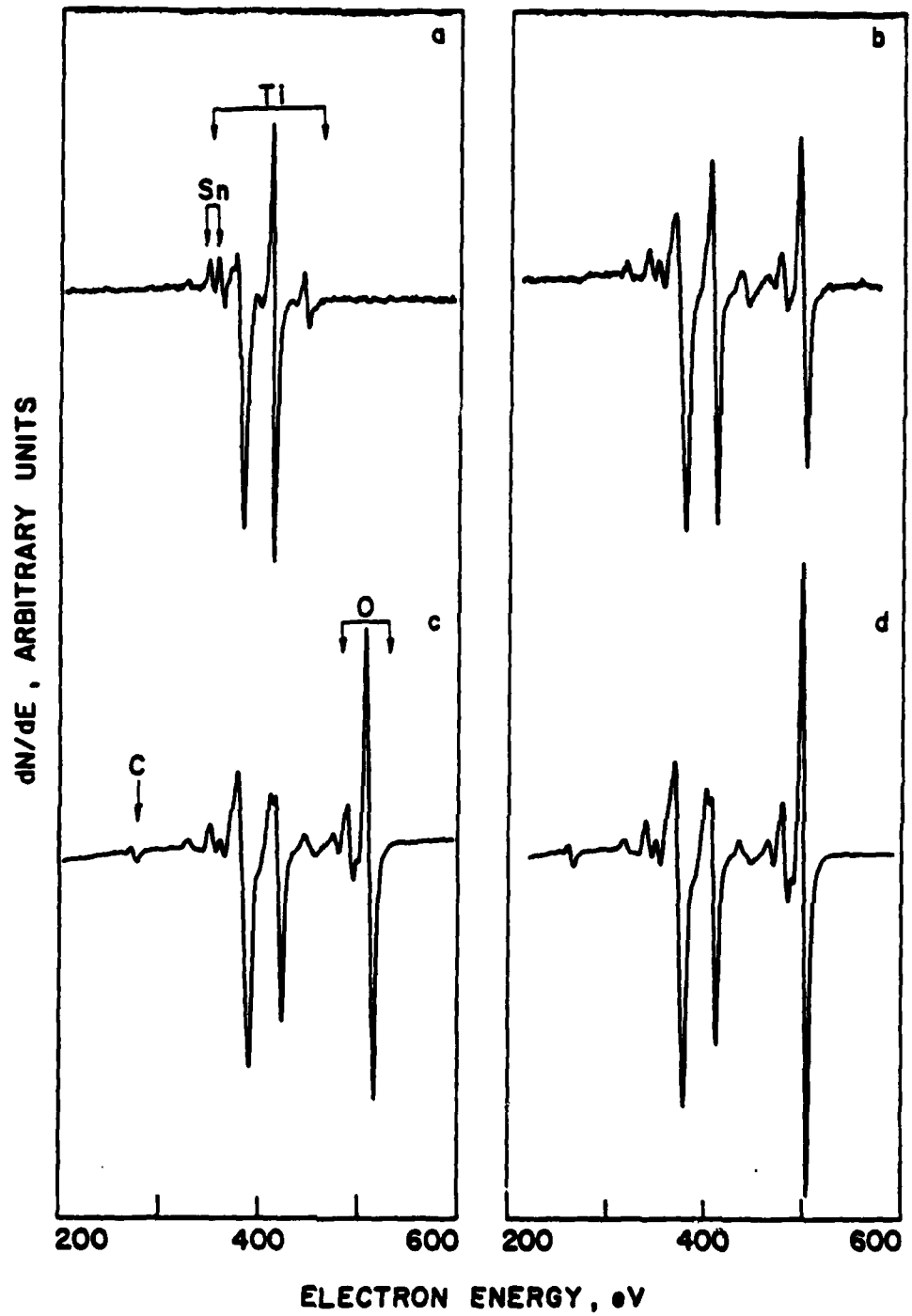

Fig. 5: Auger electron spectra of Ti-5Al-2.5Sn surfaces: (a) after impact fracture in vacuum, (b) after exposure to 5.3 x 10^{-3} Pa-s (4 x 10^{-5} torr-s) water vapor, (c) after exposure to 5.3 x 10^{-3} Pa-s (4 x 10^{-5} torr-s) oxygen, and (d) after exposure to 1.33 kPa (10 torr) water vapor. (E_p = 2 keV, 3 eV peak to peak, I_p = 20 μ A.)

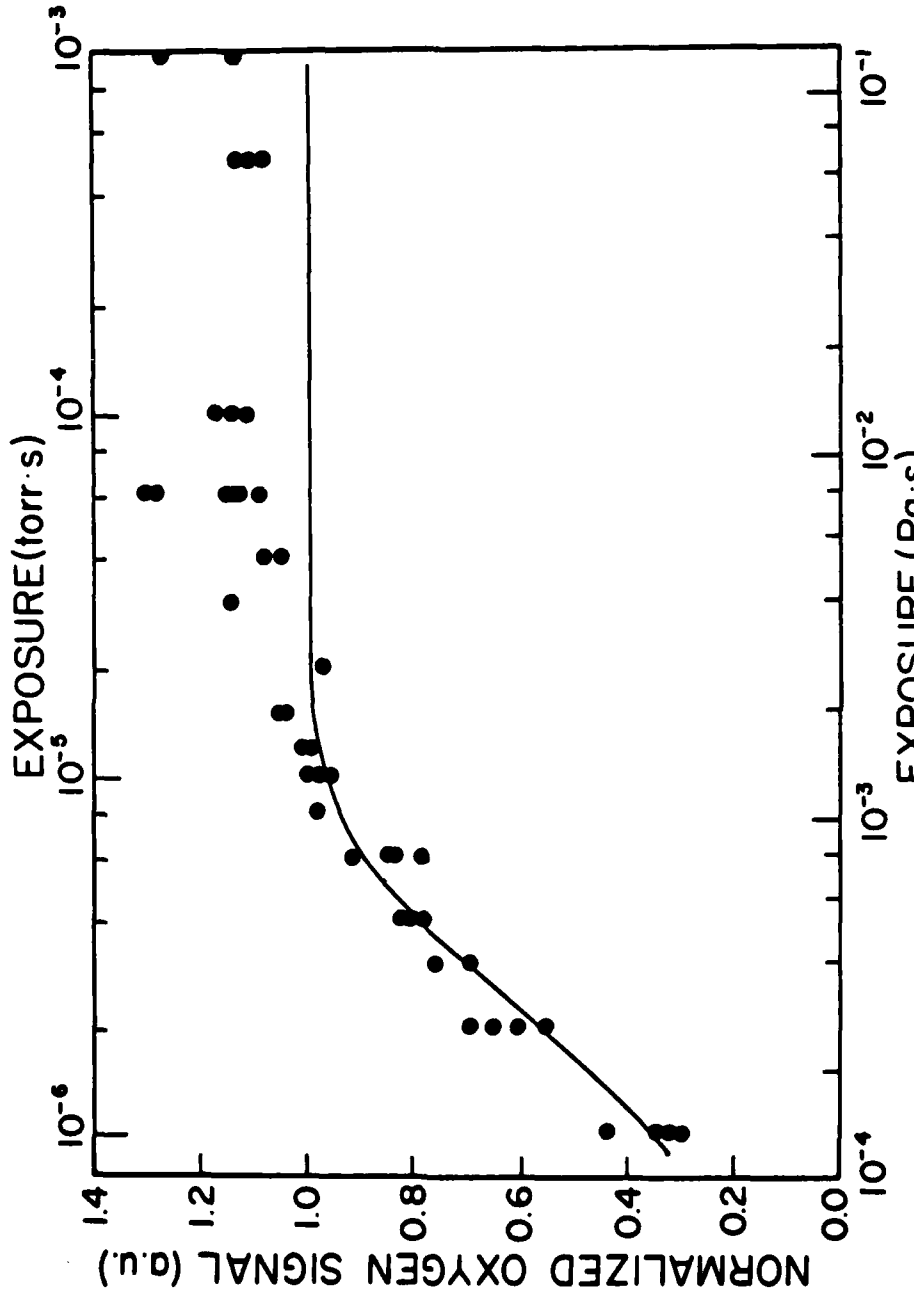

Fig. 6: Normalized oxygen Auger electron signal versus water vapor exposure.

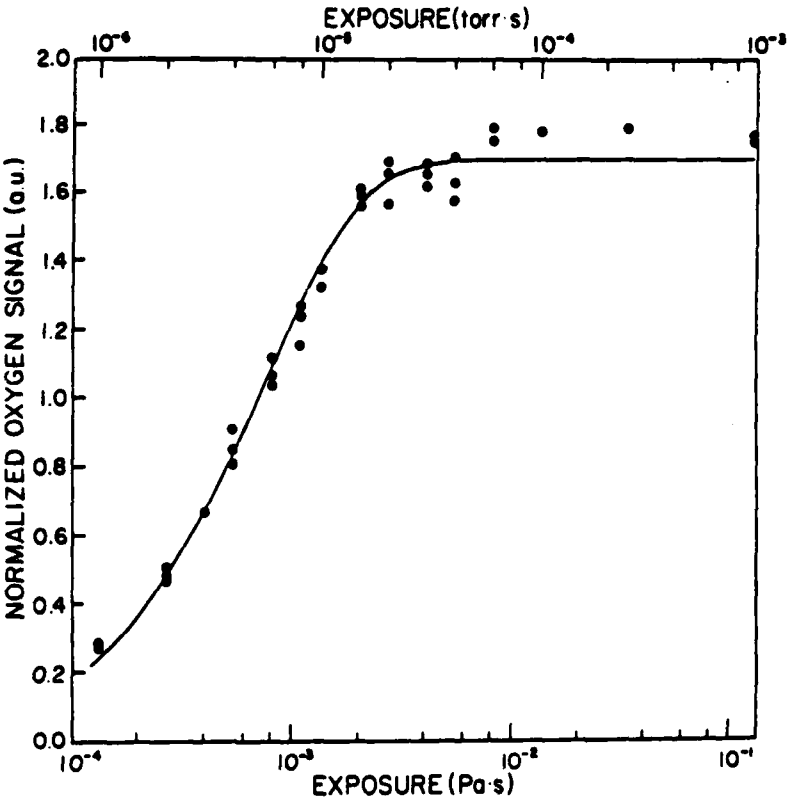

Fig. 7: Normalized oxygen Auger electron signal versus oxygen exposure.

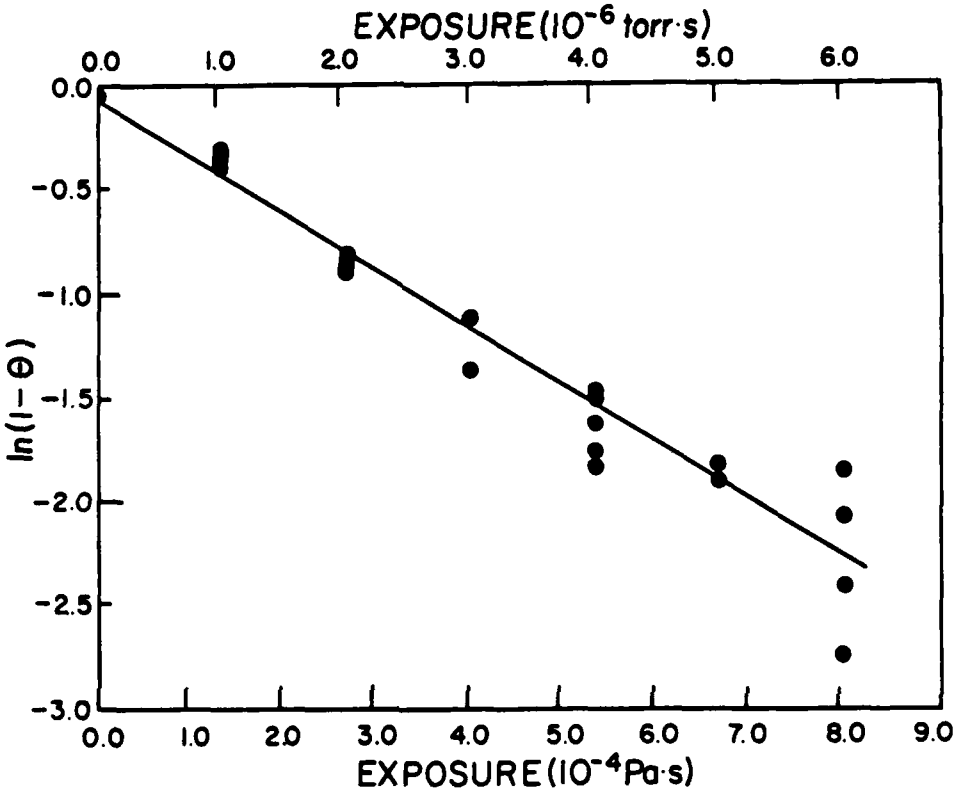

Fig. 8: Plot of ℓn (1 - θ) as a function of water vapor exposure.

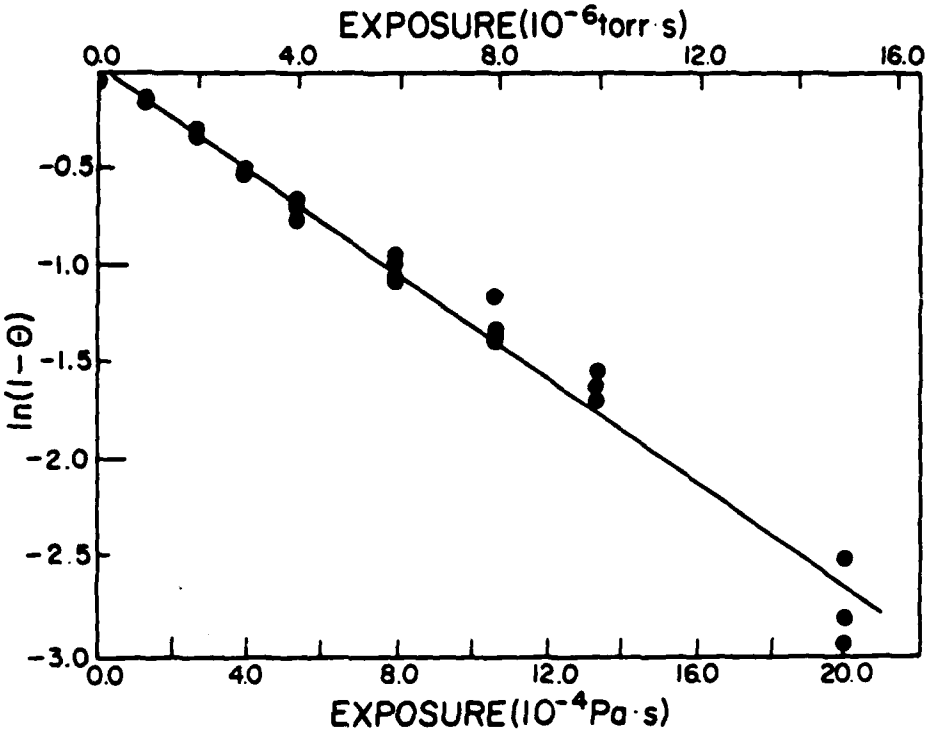

Fig. 9: Plot of ℓn (1 - θ) as a function of oxygen exposure.

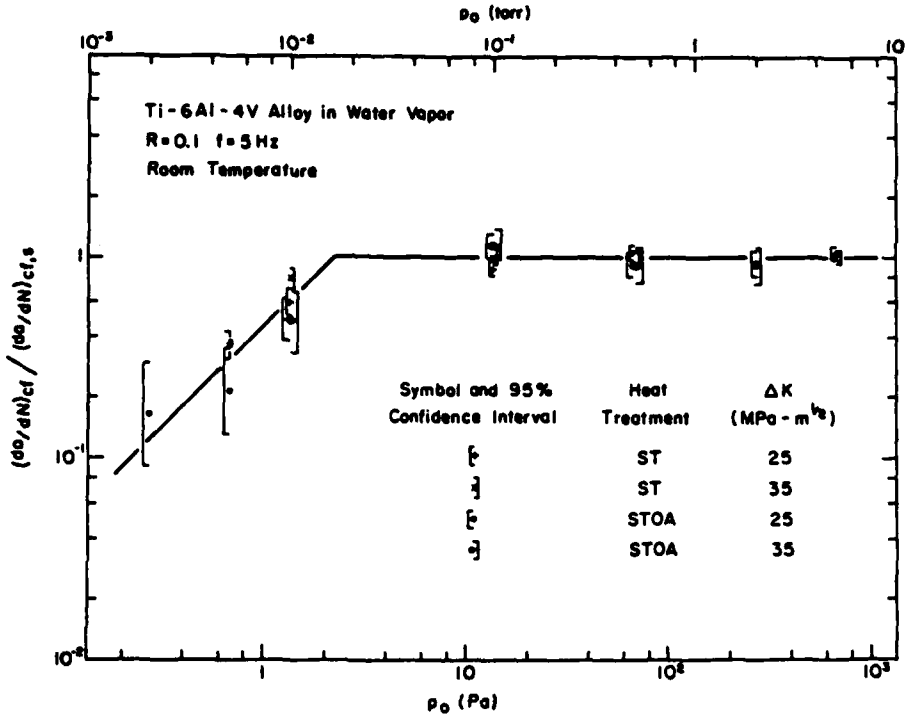

Fig. 10: Comparison of normalized (corrosion) fatigue crack growth rates for Ti-6Al-4V alloy with model predictions for pressure dependence.

BASIC DISTRIBUTION LIST

Technical and Summary Reports April 1978

Organization	Copies
Defense Documentation Center Cameron Station Alexandria, VA 22314	12
Office of Naval Research Department of the Navy 800 N. Quincy Street Arlington, VA 22217	
ATTN: Code 471	1
Code 102	1
Code 470	1
Commanding Officer Office of Naval Research Branch Office Building 114, Section D 666 Summer Street Boston, MA 02210	1
Commanding Officer Office of Naval Research Branch Office 536 South Clark Street Chicago, IL 60605	1
Office of Naval Research San Francisco Area Office One Hallidie Plaza Suite 601 San Francisco, CA 94102	1
Naval Research Laboratory Washington, DC 20375	
ATTN: Codes 6000	1
6100	1
6300	1
6400	1
2627	1
Naval Air Development Center Code 302 Warminster, PA 18964 ATTN: Mr. F. S. Williams	1

Organization	Copies
Naval Air Propulsion Test Center Trenton, NJ 08628 ATTN: Library	1
Naval Construction Batallion Civil Engineering Laboratory Port Hueneme, CA 93043 ATTN: Materials Division	1
Naval Electronics Laboratory San Diego, CA 92152 ATTN: Electron Materials Sciences Division	1
Naval Missile Center Materials Consultant Code 3312-1 Point Mugu, CA 92041	1
Commanding Officer Naval Surface Weapons Center White Oak Laboratory Silver Spring, MD 20910 ATTN: Library	1
David W. Taylor Naval Ship Research and Development Center Materials Department Annapolis, MD 21402	1
Naval Undersea Center San Diego, CA 92132 ATTN: Library	1
Naval Underwater System Center Newport, RI 02840 ATTN: Library	1
Naval Weapons Center China Lake, CA 93555 ATTN: Library	1
Naval Postgraduate School Monterey, CA 93940 ATTN: Mechanical Engineering Department	1

BASIC DISTRIBUTION LIST (cont'd)

Organization	Copies
Naval Air Systems Command Washington, DC 20360 ATTN: Codes 52031 52032	1
Naval Sea System Command Washington, DC 20362 ATTN: Code 035	1
Naval Facilities Engineering Command Alexandria, VA 22331 ATTN: Code 03	1
Scientific Advisor Commandant of the Marine Corps Washington, DC 20380 ATTN: Code AX	1
Naval Ship Engineering Center Department of the Navy Washington, DC 20360 ATTN: Code 6101	1
Army Research Office P.O. Box 12211 Triangle Park, NC 27709 ATTN: Metallurgy & Ceramics Program	1
Army Materials and Mechanics Research Center Watertown, MA 02172 ATTN: Research Programs Office	1
Air Force Office of Scientific Research Bldg. 410 Bolling Air Force Base Washington, DC 20332 ATTN: Chemical Science Directorate	1
Electronics & Solid State Sciences Directorate	1
Air Force Materials Laboratory Wright-Patterson AFB Dayton, OH 45433	1
Library Building 50, Rm 134 Lawrence Radiation Laboratory Berkeley, CA	1

Organization	Copies
NASA Headquarters Washington, DC 20546 ATTN: Code RRM	1
NASA Lewis Research Center 21000 Brookpark Road Cleveland, OH 44135 ATTN: Library	1
National Bureau of Standards Washington, DC 20234 ATTN: Metallurgy Division	1
Inorganic Materials Div.	1
Director Applied Physics Laboratory University of Washington 1013 Northeast Forthieth Street Seattle, WA 98105	1
Defense Metals and Ceramics Information Center Battelle Memorial Institute 505 King Avenue Columbus, OH 43201	1
Metals and Ceramics Division Oak Ridge National Laboratory P.O. Box X Oak Ridge, TN 37380	1
Los Alamos Scientific Laboratory P.O. Box 1663 Los Alamos, NM 87544 ATTN: Report Librarian	1
Argonne National Laboratory Metallurgy Division P.O. Box 229 Lemont, IL 60439	1
Brookhaven National Laboratory Technical Information Division Upton, Long Island New York 11973 ATTN: Research Library	1
Office of Naval Research Branch Office 1030 East Green Street Pasadena, CA 91106	1

036
16 November 1981

DISTRIBUTION LIST
Corrosion Mechanisms

Professor J. P. Hirth
Ohio State University
Department of Metallurgical Engineering
1314 Kinnear Road
Columbus, OH 43212

Dr. J. Kruger
National Bureau of Standards
Washington, DC 20234

Dr. H. K. Birnbaum
University of Illinois
Department of Metallurgy and Mining Engineering
Urbana, IL 61801

Dr. D. J. Duquette
Rensselaer Polytechnic Institute
Department of Metallurgical Engineering
Troy, NY 12181

Dr. R. P. Wei
Lehigh University
Institute for Fracture and Solid Mechanics
Bethlehem, PA 18015

Prof. H. W. Pickering
Pennsylvania State University
Department of Material Science
University Park, PA 16802

Prof. I. M. Bernstein
Carnegi-Mellon University
Schenley Park
Pittsburg, PA 15213

Dr. T. R. Beck
Electrochemical Technology Corporation
10035 31st Avenue, N.E.
Seattle, WA 98125

Prof. R. T. Foley
The American University
Washington, DC 20016

Dr. D. L. Davidson
Southwest Research Institute
8500 Culebra Road
P.O. Box Drawer 28510
San Antonio, TX 78284

Dr. Barry C. Syrett
Stanford Research Institute
333 Ravenswood Avenue
Menlo Park, CA 94025

Prof. S. Weissmann
Rutgers, The State University
of New Jersey
College of Engineering
New Brunswick, NY 08903

Prof. H. Herman
State University of New York
Material Science Department
Stony Brook, NY 11794

Prof. R. M. Latanision
Massachusetts Institute of
Technology
77 Massachusetts Avenue, Room E19-702
Cambridge, MA 02139

Prof. E. A Starke, Jr.
Dept.of Materials Science
University of Virginia
Charlottesville, VA 22901

Prof. Morris E. Fine
Northwestern University
The Technological Institute
Evanston, IL 60201

Dr. C. S. Kortovich
TRW, Inc.
2355 Euclid Avenue
Cleveland, OH 44117

Dr. O. Buck
Rockwell International Science Center
1049 Camino Dos Rios
P.O. Box 1085
Thousand Oaks, CA 91360

Dr. R. J. Arsenault
University of Maryland
College Park,MD 20742

Dr. F. Mansfeld
Rockwell International (Science Ctr)
1049 Camino Dos Rios
P.O. Box 1085
Thousand Oaks, CA 91360

Continue of Distribution List

036
16 November 1981

Dr. Paul Gordon
Illinois Institute of Technology
Department of Metallurgical and Materials
Engineering
Chicago, IL 60616

Dr. H. Leidheiser, Jr.
Lehigh University
Bethlehem, PA 18015

Dr. J. V. McArdle
University of Maryland
College Park, MD 20742

Dr. E. McCafferty
Naval Research Laboratory
Washington, DC 20375

Prof. J. G. Byrne
The University of Utah
Dept. of Materials Science & Engineering
Salt Lake City, Utah 84112

Prof. A. J. Ardell
University of California
School of Engineering and Applied Science
405 Hilgard Ave.
Los Angeles, CA 90024

Prof. J. A. S. Green
Martin Marietta Corporation
1450 South Rolling Road
Baltimore, MD 21227

Prof. G.H. Meier & F.S. Pettit
University of Pittsburgh
Dept. of Matallurgical and Materials
Engineering
Pittsburgh, PA 15261

Prof. Alexander M. Cruickshank
Gordon Research Conference
Pastore Chemical Laboratory
University of Rhode Island
Kingston, RI 02881

Dr. Theordore R. Beck
Electrochemical Technology Corp.
3935 Leary Way NW
Seattle, Washington 98107